The Astrophysical Journal, 843:105 (12pp), 2017 July 10 https://doi.org/10.3847/1538-4357/aa7893

Angular Momentum of Early- and Late-type Galaxies: Nature or Nurture?

J. Shi[1,2], A. Lapi[1,3,4], C. Mancuso[5], H. Wang[2], and L. Danese[1,3,4]
[1] SISSA, Via Bonomea 265, I-34136 Trieste, Italy
[2] Dept. of Astronomy, Univ. of Science and Technology of China, Hefei, 230026 Anhui, China
[3] INAF—Osservatorio Astronomico di Trieste, Via Tiepolo 11, I-34131 Trieste, Italy
[4] INFN—Sezione di Trieste, Via Valerio 2, I-34127 Trieste, Italy
[5] INAF—IRA, Via P. Gobetti 101, I-40129 Bologna, Italy
Received 2017 March 19; revised 2017 June 2; accepted 2017 June 7; published 2017 July 11

Abstract

We investigate the origin, shape, scatter, and cosmic evolution of the observed relationship between specific angular momentum $j_\star$ and the stellar mass $M_\star$ in early-type galaxies (ETGs) and late-type galaxies (LTGs). Specifically, we exploit the observed star formation efficiency and chemical abundance to infer the fraction $f_{\rm inf}$ of baryons that infall toward the central regions of galaxies where star formation can occur. We find $f_{\rm inf} \approx 1$ for LTGs and $\approx$0.4 for ETGs with an uncertainty of about 0.25 dex, consistent with a biased collapse. By comparing with the locally observed $j_\star$ versus $M_\star$ relations for LTGs and ETGs, we estimate the fraction f_j of the initial specific angular momentum associated with the infalling gas that is retained in the stellar component. For LTGs, we find $f_j \approx 1.11^{+0.75}_{-0.44}$, in line with the classic disk formation picture; for ETGs, we infer $f_j \approx 0.64^{+0.20}_{-0.16}$, which can be traced back to a $z \lesssim 1$ evolution via dry mergers. We also show that the observed scatter in the $j_\star$ versus $M_\star$ relation for both galaxy types is mainly contributed by the intrinsic dispersion in the spin parameters of the host dark matter halo. The biased-collapse plus merger scenario implies that the specific angular momentum in the stellar components of ETG progenitors at $z \sim 2$ is already close to the local values, in good agreement with observations. All in all, we argue that such a behavior is imprinted by nature and not nurtured substantially by the environment.

Key words: galaxies: elliptical and lenticular, cD – galaxies: evolution – galaxies: formation – galaxies: fundamental parameters

1. Introduction

The relevance of the angular momentum issue in galaxy formation and evolution has been recently reassessed by Romanowsky & Fall (2012) and Fall & Romanowsky (2013), who critically reviewed previous results and pointed out the still-open problems and the main perspectives toward solving them.

In fact, the origin of angular momentum in galaxies has been hotly debated for a long time, well before the establishment of the modern cold dark matter (DM) paradigm for structure formation. Hoyle (1949) first pointed out that the tidal field generated by an irregular matter distribution around a proto-galaxy may transfer to it a large amount of angular momentum. Such irregular distribution of matter is indeed expected to develop and operate as a consequence of gravitational instability (see Sciama 1955; Peebles 1969; Doroshkevich 1970; White 1984). This idea was then successfully applied to compute the angular momentum acquired by galactic DM halos in the context of the standard cosmological framework (e.g., Catelan & Theuns 1996).

On the observational side, Takase & Kinoshita (1967) and Freeman (1970) investigated the relationship between the total angular momentum $J_\star$ of the stellar disk and the stellar mass $M_\star$ for local spiral galaxies, finding a power-law behavior with a slope of $\approx 7/4$. Fall (1983) pointed out that a more relevant quantity is constituted by the specific angular momentum $j_\star = J_\star/M_\star$, given by the product of a length scale and a rotational velocity. He also showed that both spiral and elliptical galaxies follow a $j_\star$ versus $M_\star$ relation with a similar slope of $\approx$0.6, but with the former exhibiting systematically larger values of $j_\star$ by a factor of $\approx$5.

The angular momentum of spiral and elliptical galaxies, considered in connection with their structural properties and the angular momentum of their host DM halos, became and still remains a key aspect of galaxy formation and evolution (e.g., Efstathiou & Jones 1979, 1980; Davies & Illingworth 1983; Mo et al. 1998; van den Bosch et al. 2001; Dutton & van den Bosch 2012; Burkert et al. 2016; for a textbook, see Mo et al. 2010; Del Popolo 2016). Fall & Efstathiou (1980) discussed the origin of the rotational properties in disk galaxies within DM halos by comparing the expectations from the theoretical framework outlined by White & Rees (1978) to the available data.

The favored scenario for late-type galaxies (LTGs) envisages that the specific angular momentum of the material forming the disk mirrors that of the host DM halo (see Fall & Efstathiou 1980; Fall 1983; Mo et al. 1998). Such an assumption is indeed endorsed by the results of more recent numerical simulations (e.g., Governato et al. 2007; Zavala et al. 2016; Lagos et al. 2017). However, galaxy outflows and tidal stripping have also been advocated in order to rearrange the observed angular momentum in LTGs with different bulges over a total mass ratio B/T (see Maller & Dekel 2002; Brook et al. 2012; Dutton & van den Bosch 2012; Sharma et al. 2012).

By contrast, the origin of the low angular momentum measured in early-type galaxies (ETGs) is still open to debate, with a particular focus on the role of merging processes (e.g., Hopkins et al. 2009) versus disk instabilities (e.g., Shlosman & Noguchi 1993; Noguchi 1999; Immeli et al. 2004a, 2004b; Bournaud et al. 2007; for a review, see Bournaud 2016) as possible mechanisms to transfer and/or lose angular momentum.

An original approach to the issue of angular momentum in galaxy formation has been sketched by Eke et al. (2000) and

Fall (2002), starting from the well-known fact that only a fraction $f_{\rm inf}$ of the baryons associated with the DM halo are eventually found in the luminous components of galaxies, namely, stars, the interstellar medium (ISM), and dust (see Persic & Salucci 1992; Fukugita et al. 1998). Then, it is reasonable to envisage that only the gas in the inner regions undergoes collapse and fuels star formation, while the outer portions of the galaxy are somehow refrained from forming stars. Since the specific angular momentum of the host DM halo decreases toward the inner regions (e.g., Bullock et al. 2001), the stars formed there should exhibit a lower $j_\star$. Romanowsky & Fall (2012) put forward this "biased collapse" scenario and analyzed its merits and drawbacks.

In the present paper, we show that the infall fraction $f_{\rm inf}$ that provides a quantitative description of the biased collapse scenario can be inferred from observations of the star formation efficiency and chemical abundance of galaxies. The data indicate that the fraction $f_{\rm inf}$ is appreciably different for ETGs and LTGs, implying that the two galaxy types occupy distinct loci in the specific angular momentum versus stellar mass diagram. As a consequence, ETGs and LTGs are found to have retained in their stellar components a different fraction f_j of the angular momentum initially associated with the infalling baryons. We estimate such quantities and discuss how to physically interpret them in light of a biased-collapse plus merger scenario.

The plan of the paper is as follows. After a brief presentation of the argument (Section 2), in Section 3, we show how to infer a robust estimate of the infalling gas fraction as a function of the stellar mass for both ETGs and LTGs by exploiting their observed star formation efficiency and metal abundance. Section 4 is devoted to presenting and summarizing the available data on star formation efficiency and metallicity in ETGs and LTGs. The infalling gas fraction and its impact on the specific angular momentum of both galaxy types are investigated in Section 5. In Section 6, we discuss our results and compare them with recent observational data and numerical simulations. Section 7 summarizes our key findings.

Throughout this work, we adopt the standard flat cosmology from Planck Collaboration et al. (2016) with round parameter values: matter density $\Omega_M = 0.31$, baryon density $\Omega_b = 0.05$, Hubble constant $H_0 = 100\,h\,{\rm km\,s^{-1}\,Mpc^{-1}}$ with $h = 0.67$, and mass variance $\sigma_8 = 0.83$ on a scale of $8\,h^{-1}$ Mpc. Stellar masses and star formation rates (or luminosities) of galaxies are evaluated assuming the Chabrier (2003) initial mass function (IMF).

2. The Initial Specific Angular Momentum of Inflowing Gas

The galaxy angular momentum acquired by proto-galaxies is classically presented in terms of the dimensionless spin parameter

$$\lambda \equiv \frac{J\,|E|^{1/2}}{G\,M^{5/2}}, \tag{1}$$

which is a combination of basic galactic physical quantities, namely, the total angular momentum J, the total energy E, and the total mass M (DM and baryons; see Peebles 1969, 1971). The distribution of the spin parameter as a function of mass, redshift, and environment has been studied with both analytic approximations and numerical simulations (e.g., Barnes & Efstathiou 1987; Bett et al. 2007; Macciò et al. 2007; Rodríguez-Puebla et al. 2016; Wang & Kang 2017). The emerging picture envisages that the halo spin parameter exhibits a lognormal distribution with average $\langle\lambda\rangle \approx 0.035$ and dispersion $\sigma_{\log\lambda} \approx 0.25$ (Rodríguez-Puebla et al. 2016), nearly independent of mass and redshift but somewhat dependent on environment (e.g., Bett et al. 2007; Macciò et al. 2007, 2008; Shi et al. 2015). After Romanowsky & Fall (2012), we can define the specific angular momentum $j \equiv J/M$ of a spherically symmetric DM halo with mass distribution following a Navarro–Frenk–White (NFW) profile (Navarro et al. 1996, 1997) extended out to the conventional virial radius $r_{\rm vir}$,

$$j(r_{\rm vir}) \approx 4.2 \times 10^4 \lambda \left(\frac{M_{\rm vir}}{10^{12}\,M_\odot}\right)^{2/3} \times E(z)^{-1/6}\,{\rm km\,s^{-1}\,kpc}, \tag{2}$$

where $E(z) \equiv \Omega_\Lambda + \Omega_M (1+z)^3$. Note that the redshift dependence is weak; for instance, a halo at $z \approx 2$ features a momentum $j(r_{\rm vir})$ lower by a relatively small factor of $\approx$1.4 than that of a halo with the same mass at $z = 0$.

Barnes & Efstathiou (1987) and Bullock et al. (2001) pointed out via N-body simulations that the radial distribution of the halo specific angular momentum is well described by a power law with exponent $s \approx 1$, i.e.,

$$j(r) = j(r_{\rm vir}) \left[\frac{M(\leqslant r)}{M(\leqslant r_{\rm vir})}\right]^s, \tag{3}$$

implying that the inner regions of halos exhibit a lower specific angular momentum than the outer ones. In Appendix A, we exploit state-of-the-art, high-resolution N-body simulations to derive the distribution of the parameter s as a function of mass and redshift (see also Figures 6 and 7).

Next, we assume that the baryonic mass initially follows the same radial distribution of the DM with ratio $f_b \equiv M_b/M_{\rm vir} = \Omega_b/\Omega_M$; thus, the distributions of specific angular momentum for the baryonic gas $j_b(r)$ and the DM $j(r)$ mirrors each other, i.e., $j_b(r) = j(r)$. However, it could happen that only a fraction $f_{\rm inf}$ of the baryons associated with the galaxy halo are able to cool down and flow inward to reach the inner regions, where most of the star formation occurs. Then, such baryons are expected to feature a specific angular momentum lower than $j_{\rm vir}$. Providing more detail, after Equation (3), the fraction of baryons involved in the formation of the galaxy $f_{\rm inf} \equiv M_{\rm inf}/f_b\,M_{\rm vir} = M_b(\leqslant r_{\rm inf})/M_b(\leqslant r_{\rm vir}) \leqslant 1$ has an initial specific angular momentum

$$j_{\rm inf} = j(r_{\rm vir}) f_{\rm inf}^s\,. \tag{4}$$

Note that this equation is very similar in spirit to Equation (14) by Fall (1983), who advocated tidal stripping as a possible mechanism to prevent baryons in the outer regions of halos hosting ETGs collapse.

As we see below (Sections 4.1 and 4.3), the halo mass for galaxies endowed with stellar mass $M_\star$ can be estimated via various techniques. The outcome is usually expressed in terms of the star formation efficiency $f_\star \equiv M_\star/f_b\,M_{\rm vir}$ as a function of the stellar mass $M_\star$. Plugging the definition of $f_\star$ into Equations (2) and (4), we can write the intrinsic angular momentum of the inflowing gas as a function of the stellar

mass and star formation efficiency,

$$j_{\rm inf} \approx 3.1 \times 10^4\, \lambda\, f_\star^{-2/3} \left(\frac{M_\star}{10^{11}\, M_\odot}\right)^{2/3} \times f_{\rm inf}^{s}\; E(z)^{-1/6}\ {\rm km\ s^{-1}\ kpc}. \quad (5)$$

The above formula differs from Equation (15) of Romanowsky & Fall (2012) in two respects: (i) we introduce the dependence on redshift (see also Burkert et al. 2016), and (ii) we focus on the specific angular momentum of the infalling gas. By comparing the observed $j_\star$ to $j_{\rm inf}$, we aim to determine the fraction $f_j \equiv j_\star/j_{\rm inf}$ of the initial specific angular momentum retained by the stellar component (see Romanowsky & Fall 2012).

The next section is devoted to developing a method aimed at estimating the infalling baryon fraction $f_{\rm inf}$ from the observed star formation efficiency and metal abundance for both ETGs and LTGs.

3. Fraction of Inflowing Gas from Stellar Efficiency and Metal Abundance

In the local universe, most of the baryonic mass within the central region (size $\lesssim$10–20 kpc) of galaxies comprises three main components: stars, dust, and the ISM. An additional diffuse component of warm/hot gas, often dubbed the circumgalactic medium (CGM; e.g., Tumlinson et al. 2011), pervades a much larger volume up to hundreds of kpc. These components descend from the diffuse gas of mass M_b associated with the galactic halo at the epoch of halo virialization. A portion (or all) of the gas cools down from the initial virial temperature, allowing star formation to occur (especially in clumpy regions) and chemical enrichment of the galactic components to proceed. A fraction of the cooled gas can eventually be expelled from the central regions by energy/momentum feedback associated with supernova explosions/stellar winds and outbursts from the central active galactic nucleus (AGN). This feedback, depending on the history of star formation and AGN accretion, can be so efficient as to quench star formation and forbid further cooling of the hot/warm gas (see White & Frenk 1991; Bressan et al. 1998; Cole et al. 2000). This is particularly true for AGNs, which are indeed expected to originate large-scale outflows (see Granato et al. 2004; Di Matteo et al. 2005; Lapi et al. 2006). Statistical evidence of the latter can be recognized in the chemical enrichment of the intracluster medium (e.g., Leccardi et al. 2010; Böhringer 2014).

The total mass of the observed baryonic components—namely, the mass in stars $M_\star$ (including stellar remnants), ISM $M_{\rm ISM}$, dust $M_{\rm dust}$, and CGM $M_{\rm CGM}$—should not exceed the mass M_b of the baryons associated with the galaxy halo. By Meanwhile, the balance of the baryonic mass that cools and infalls toward the central regions $M_{\rm inf}$, the mass of the baryons still in the galaxy $M_{\rm gal} = M_\star + M_{\rm ISM} + M_{\rm dust}$, and the mass $M_{\rm out}$ of the gas expelled from the central regions by feedback mechanisms can be written as

$$M_{\rm gal} \equiv M_{\rm inf} - M_{\rm out}; \quad (6)$$

note that the CGM does not enter the galaxy mass balance. As for the budget of metals, Fukugita & Peebles (2004) have shown that most of them are locked up in compact objects, such as white dwarfs, neutron stars, and stellar mass black holes. However, here we are interested in the budget of metals produced by stars but not locked up in their compact remnants; we denote these as accessible metals. Observations of stellar metallicity in galaxies essentially refer to that of main-sequence stars after proper luminosity weighting.

In order to evaluate the accessible metals produced in a galaxy, a relevant quantity is constituted by the true metal yield y_Z of a single stellar population. Here, we adopt the classic definition of y_Z that includes a normalization to $1 - R$, where R is the return fraction of gaseous material from the formed stars (e.g., Vincenzo et al. 2016). In the following, we assume instantaneous recycling, but we have checked with detailed chemical evolution models that this is indeed a good approximation in our context (see also Feldmann 2015; Vincenzo et al. 2016). Note that y_Z depends on the assumed Chabrier IMF and mildly on the chemical composition of the stars. However, for our purposes, this is a second-order effect, so we just exploit the average yields appropriate for reasonable chemical abundances (e.g., Peeples et al. 2014; Feldmann 2015; Vincenzo et al. 2016). Under these assumptions, the total mass of accessible metals produced by stars is

$$M_Z = y_Z\, M_\star, \quad (7)$$

where $y_Z \approx 0.069$ applies for a Chabrier IMF (Krumholz & Dekel 2012).

The budget of accessible metals inside the galaxy reads

$$\begin{aligned} M_{Z,\rm gal} &= M_{Z,\star} + M_{Z,\rm ISM} + M_{Z,\rm dust} \\ &= \langle Z_\star \rangle M_\star + \langle Z_{\rm ISM} \rangle M_{\rm ISM} + M_{\rm dust}, \end{aligned} \quad (8)$$

where we set $M_{Z,\star} = \langle Z_\star \rangle M_\star$, $M_{Z,\rm ISM} = \langle Z_{\rm ISM} \rangle M_{\rm ISM}$, and $M_{Z,\rm dust} = M_{\rm dust}$, i.e., $\langle Z_{\rm dust} \rangle = 1$. The metal mass conservation implies (see, e.g., Peeples et al. 2014)

$$M_Z = M_{Z,\rm gal} + M_{Z,\rm out}, \quad (9)$$

where $M_{Z,\rm out} = \langle Z_{\rm out} \rangle M_{\rm out}$ is the mass of metals expelled from the galaxy and disseminated in the CGM and IGM (see Peeples et al. 2014). The above equation assumes that (i) the cool gas inflowing from the galactic halo has a negligible metal content and (ii) outflowing mass and metals do not fall back at later times (i.e., no circulation due to a galactic fountain). We discuss in Appendix B how relaxing such assumptions does not appreciably alter our results and conclusions.

Replacing $M_{\rm out}$ and $M_{Z,\rm gal}$ after Equations (6) and (8), we get

$$\begin{aligned} y_Z\, M_\star = &\langle Z_\star \rangle\, M_\star + \langle Z_{\rm ISM} \rangle M_{\rm ISM} + M_{\rm dust} \\ &+ \langle Z_{\rm out} \rangle\, (M_{\rm inf} - M_\star - M_{\rm ISM} - M_{\rm dust}). \end{aligned} \quad (10)$$

Then, we express the average metal abundance of the outflowing gas in terms of the stellar metallicity via the parameter $\zeta \equiv \langle Z_{\rm out} \rangle / \langle Z_\star \rangle$ and insert the star formation efficiency $f_\star \equiv M_\star/f_b\, M_{\rm vir}$ and infall fraction $f_{\rm inf} \equiv M_{\rm inf}/f_b\, M_{\rm vir}$ to obtain

$$f_{\rm inf} = f_\star \left(\frac{y_Z}{\zeta\, \langle Z_\star \rangle} - \frac{M_{Z,\rm gal}}{\zeta\, \langle Z_\star \rangle M_\star} + \frac{M_{\rm gal}}{M_\star} \right). \quad (11)$$

We can infer ζ from general arguments. In the case of feedback originated by stellar winds and supernova explosions, the outflow rate is proportional to the star formation rate $\dot{M}_{\rm out} \approx \epsilon_{\rm out}\, \dot{M}_\star$, where $\epsilon_{\rm out}$ is the mass loading factor. Then, $M_{\rm out}(\tau) \approx \epsilon_{\rm out}\, M_\star(\tau)$ holds at any galactic age τ (e.g., Feldmann 2015), implying that

both the stellar metallicity $Z_\star$ and the outflow metallicity $Z_{\rm out}$ can be computed as

$$Z_X(\tau) = \frac{1}{M_X(\tau)} \int_0^\tau d\tau' Z_{\rm gas}(\tau')\dot{M}_X(\tau'), \quad (12)$$

with $X = \star$ or $X =$ out. As a consequence, the metallicities of the stars and outflows are quite close to each other, $Z_{\rm out}(\tau) \approx Z_\star(\tau)$. Therefore, for galaxies with outflows dominated by stellar feedback, e.g., LTGs, $\zeta \approx 1$ applies.

By contrast, the effect of the AGN feedback, relevant in the case of ETGs, can simply be described as an abrupt quenching of star formation, where most of the gas is assumed to be removed. If the feedback occurs at time $\tau_{\rm AGN}$, then the metallicity reads

$$Z_{\rm out} = \frac{M_{Z,\rm out}}{M_{\rm out}} = \frac{Z_\star(\tau_{\rm AGN})\epsilon_{\rm out}M_\star(\tau_{\rm AGN}) + Z_{\rm gas}(\tau_{\rm AGN})M_{\rm gas}(\tau_{\rm AGN})}{\epsilon_{\rm out}\,M_\star(\tau_{\rm AGN}) + M_{\rm gas}(\tau_{\rm AGN})}. \quad (13)$$

Since the gas metallicity $Z_{\rm gas}$ is increasing with time, Equation (12) implies that the metal abundance of the stars is lower than that of the gas for small galactic age $\tau \ll 10^8$ yr, but they converge, $Z_{\rm gas}(\tau) \approx 1.1\,Z_\star(\tau)$, after a few 10^8 yr. As a result, $Z_{\rm out} \approx Z_\star$ also holds in the case of AGN feedback. Summing up, we conclude that $\zeta \approx 1$ applies for both ETGs and LTGs.

4. Star Formation Efficiency and Metallicity of ETGs and LTGs

In this section, we examine the star formation efficiency (or, equivalently, the stellar-to-halo mass ratio) and metal abundance in ETGs and LTGs.

The host halo mass of galaxies has been investigated by exploiting different observational approaches and theoretical assumptions; the more common techniques involve satellite kinematics, weak gravitational lensing, and abundance matching. Satellite kinematics and weak lensing offer the important opportunity to separately study ETGs and LTGs (e.g., More et al. 2011; Wojtak & Mamon 2013; Velander et al. 2014; Hudson et al. 2015; Mandelbaum et al. 2016). In particular, weak lensing has been exploited to investigate large samples of galaxies via stacking techniques, even at significant redshift $z \lesssim 0.7$ (e.g., Hudson et al. 2015). Abundance matching also provides insights on the galaxy-to-halo mass ratio at substantial redshift (e.g., Shankar et al. 2006; Behroozi et al. 2010, 2013; Moster et al. 2013; Aversa et al. 2015; Huang et al. 2017), although the separation between galaxy types is more challenging.

4.1. Star Formation Efficiency of ETGs

In Figure 1 (top panel), we present the star formation efficiency of ETGs as a function of their stellar mass for relatively local samples at $z \lesssim 0.3$. Data are from recent estimates based on satellite kinematics (More et al. 2011; Wojtak & Mamon 2013), weak lensing (Velander et al. 2014; Hudson et al. 2015; Mandelbaum et al. 2016), and abundance matching (Rodríguez-Puebla et al. 2015). Most data refer to the central/brightest red galaxy of a halo, possibly corrected for the contribution from satellites. This procedure is quite complex and

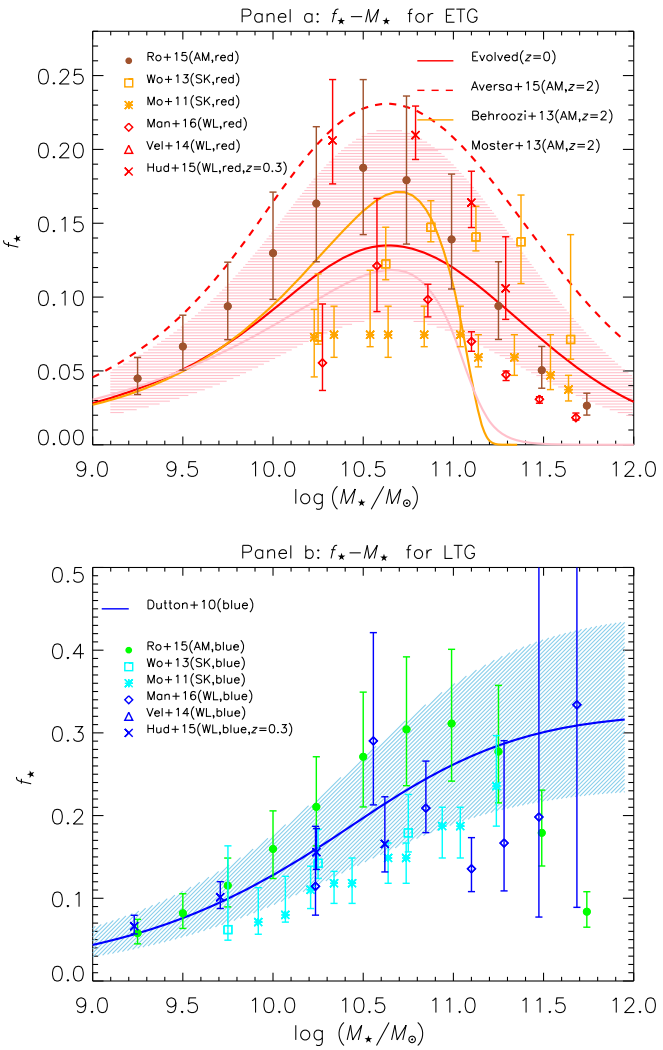

Figure 1. Star formation efficiency $f_\star$ vs. stellar mass $M_\star$ for ETGs (top panel) and LTGs (bottom panel). Top panel: the red dashed line represents the relationship at $z = 2$ for ETGs inferred from Aversa et al. (2015) via the abundance-matching technique, while the red solid line is the same relationship evolved to $z = 0$ (see details in Section 4.1), with the red shaded area showing the 1σ uncertainty. The orange and pink lines are the abundance-matching results at $z = 2$ from Behroozi et al. (2013) and Moster et al. (2013), respectively. Filled circles are the abundance-matching data for red galaxies at $z = 0$ from Rodríguez-Puebla et al. (2015). Other data points are weak lensing or satellite kinematic measurements in the local universe from Wojtak & Mamon (2013), More et al. (2011), Mandelbaum et al. (2016), Velander et al. (2014), and Hudson et al. (2015) at $z = 0.3$. Bottom panel: the blue solid line represents the $f_\star$ vs. $M_\star$ relation for LTGs from Dutton et al. (2010), with the blue shaded area indicating the 1σ uncertainty. Data are from the weak lensing and satellite kinematic observations cited above, but for blue galaxies.

can significantly contribute to the observed scatter of about 0.2 dex (see Behroozi et al. 2013; Reddick et al. 2013; Huang et al. 2017), as shown by the red shaded area.

Now we turn to the problem of estimating the star formation efficiency at the reference redshift/epoch when most ($\gtrsim$70%) of the stars have been formed in the ETG progenitors. The notions that ETGs are quite old systems (formation redshift $z \gtrsim 1$) and that they formed in a relatively short timescale ($\lesssim$1 Gyr) are time-honored (e.g., Bower et al. 1992; Thomas et al. 2005, 2010; for a review, see Renzini 2006). This is strongly supported by recent archeological studies on massive, passively evolving galaxies at substantial redshift $z \lesssim 1$, which show that they formed most of their stars at

$z \sim 1.5$–2 (e.g., Gallazzi et al. 2006, 2014; Trujillo et al. 2011; Choi et al. 2014; Lonoce et al. 2015; Onodera et al. 2015; Citro et al. 2016; Kriek et al. 2016; Glazebrook et al. 2017; Siudek et al. 2017). Even lower-mass ETGs formed mostly at $z \sim 1$, as pointed out by Siudek et al. (2017). We further notice that the cosmic stellar mass density increased by ≈40% from $z \approx 1$ to the present (see Madau & Dickinson 2014; Aversa et al. 2015); this increase corresponds to the present-day fraction of stellar mass density contributed by disk-dominated galaxies, including Sa (e.g., Moffett et al. 2015).

Investigations of the fraction of close galaxy pairs and galaxies with disturbed morphologies in large catalogs (e.g., Man et al. 2016) indicate that the mass growth of massive galaxies $M_\star \gtrsim 7 \times 10^{10}\,M_\odot$ is constrained within a factor of ≈1.5–2 in the redshift interval $z \sim 0.1$–2.5. Limited mass evolution $\Delta \log M_\star \approx 0.16 \pm 0.04$ is also confirmed for a sample of quiescent galaxies at redshift $z \lesssim 1.6$ by Belli et al. (2014).

In the following, we assume for ETGs a reference formation (when ≳70% of the stars have been formed) redshift $z \approx 2$ and an average stellar mass increase of 50% since then. Because the stellar mass function at $z \approx 2$ is mainly dominated by the ETG progenitors, it is reasonable for us to exploit the abundance-matching technique applied to galaxies at $z \approx 2$ in order to derive an estimation of the star formation efficiency in ETG progenitors.

In Figure 1 (top panel), we present the outcome of the abundance matching at $z \approx 2$ between the stellar and halo mass functions computed by Aversa et al. (2015). The results from Moster et al. (2013) and Behroozi et al. (2013) are also shown for comparison. The resulting star formation efficiencies differ by no more than a factor of 2. A relevant check on the efficiency can be done by comparing the estimate at $z \approx 2$ to the low-redshift estimates based on weak lensing and satellite kinematics. Evolution in both halo and stellar mass must be taken into account. For the stellar mass change, we assume an increase of 50%, as mentioned above.

The halo mass evolution has been computed via *N*-body simulations by McBride et al. (2009) and Fakhouri et al. (2010) and the excursion set approach by Lapi et al. (2013), with concordant results. The main progenitor of a present-day halo with virial mass $M_{\rm vir}$ evolves from $z \approx 2$ to the present as

$$M_{\rm vir}(z=0) \approx 4.0\, M_{\rm vir}(z=2)\left[\frac{M_{\rm vir}(z=0)}{10^{14}\,M_\odot}\right]^{0.12}. \qquad (14)$$

The solid red line in Figure 1 shows how the star formation efficiency estimated by Aversa et al. (2015) at $z \approx 2$ evolves toward $z \approx 0$ along the assumed evolutionary pattern for DM and stellar mass. The agreement with local data derived from weak gravitational lensing and satellite kinematics is good. We also checked that the proposed evolution is similar to that inferred by Hudson et al. (2015) for red galaxies with stellar mass $M \gtrsim 2 \times 10^{10}\,M_\odot$ (in our framework ETGs) between $z \approx 0.7$ and 0.3. Therefore, we adopt the estimation from Aversa et al. (2015) as the star formation efficiency for $z = 2$ ETG progenitors.

4.2. Metal Abundance of ETGs

In order to derive the inflowing gas fraction $f_{\rm inf}$ from Equation (11), not only the star formation efficiency $f_\star$ but also the stellar metallicity $Z_\star$ at $z \approx 2$ is needed.

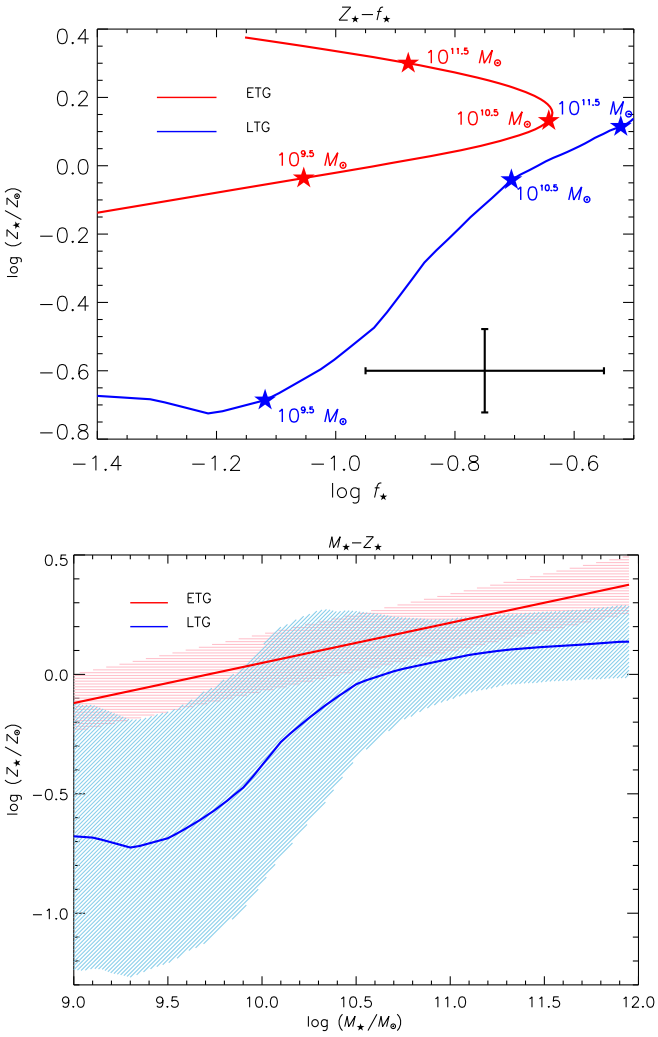

Figure 2. Top panel: stellar metallicity $Z_\star$ (in units of the solar value $Z_\odot = 0.015$) plotted against star formation efficiency $f_\star$ for ETGs (red) and LTGs (blue). The stars highlight the positions on the curves for galaxies with stellar masses $M_\star \approx 10^{9.5}$–$10^{10.5}$–$10^{11.5}\,M_\odot$. The error bars in the bottom right corner indicate the typical uncertainty in the measurements of $Z_\star$ and $f_\star$. Bottom panel: stellar metallicity $Z_\star$ vs. $M_\star$ for ETGs (red) and LTGs (blue), taken from Gallazzi et al. (2005, 2006). The red and blue shaded areas show the 1σ uncertainty.

As for the stellar metallicity of ETGs, we adopt the relationship $Z_\star$ versus $M_\star$ proposed by Gallazzi et al. (2006) for a local $z \lesssim 0.2$ galaxy sample with its 1σ scatter of 0.12 dex (red line and red shaded area in the bottom panel of Figure 2). There is evidence that, after the main burst of star formation, the metal abundance of stars in ETGs stays practically constant (e.g., Choi et al. 2014; Gallazzi et al. 2014; Citro et al. 2016; Siudek et al. 2017), as confirmed from high-redshift observations of passively evolving galaxies (see Lonoce et al. 2015; Kriek et al. 2016). Therefore, we reasonably assume that the present-day metallicity of massive ETGs was already in place at redshift $z \approx 2$. For ETGs, we also neglect both dust and the ISM in the mass and metals budget.

4.3. Star Formation Efficiency of LTGs

By comparing the panels of Figure 1, it is apparent that local LTGs exhibit a larger star formation efficiency than ETGs. In particular, at high stellar masses, LTGs appear more efficient by a factor of 1.5–2 (see Dutton et al. 2010; More et al. 2011;

Wojtak & Mamon 2013; Velander et al. 2014; Rodríguez-Puebla et al. 2015; Mandelbaum et al. 2016). Despite the large scatter of the data, a higher efficiency for LTGs is found from several samples, independent of whether the halo mass is derived via abundance matching or weak lensing. In the bottom panel of Figure 1, we illustrate the fit to the data by Dutton et al. (2010) with its associated 1σ uncertainty, shown by the blue shaded area.

At variance with ETGs, Hudson et al. (2015) showed that the relationship between efficiency and stellar mass does not appreciably evolve between $z \approx 0.7$ and 0.3. A straightforward interpretation is that, in LTGs, the star formation and DM accretion are parallel along cosmic times. In the following, we assume that the star formation efficiency versus stellar mass relationship in LTGs stays almost constant, close to the present-day value, along the period of disk formation.

4.4. Metal Abundance of LTGs

In the case of LTGs, the mass in the ISM and dust is no more negligible, and, as a consequence, they can contribute significantly to the global galaxy metal abundance. The amount of stars, ISM, and dust and their metal abundance have been presented by Peeples et al. (2014). We adopt their relationships with the associated scatter and refer the reader to their paper for details. Note that the stellar metallicity measurements still retain an appreciable uncertainty (Gallazzi et al. 2005; Goddard et al. 2017), especially for low-mass LTGs (cf. bottom panel of Figure 2). Another caveat concerns the metal mass in the ISM, which includes only cold gas in the analysis of Peeples et al. (2014); the mass and metals in warm ionized gas could be as large as those in the cold gas (see Sembach et al. 2000; Haffner et al. 2009; Peeples et al. 2014). We checked that doubling the ISM mass and metals only marginally affects our results; e.g., the infall fraction $f_{\rm inf}$ (cf. Section 5) changes by no more than 10%.

We recall that LTGs are still forming stars in their disks at exponentially declining rates (e.g., Chiappini et al. 1997). This implies that the metallicity increases along cosmic times. The median increase from $z \approx 0.7$ to the present has been estimated by Gallazzi et al. (2014) to be $\lesssim$0.12 dex, which is comparable to the uncertainties in the metallicity estimates (see Gallazzi et al. 2005; Peeples et al. 2014).

5. Estimated Fraction of Inflowing Gas and Specific Angular Momentum

Figure 2 shows that ETGs and LTGs occupy different loci in the $f_\star$ versus $Z_\star$ plane. At a given metallicity, the efficiency is higher for LTGs; by contrast, ETGs feature higher metallicity even if the efficiency is small. These observational results directly impact the fraction $f_{\rm inf}$ of gas flowing into the central regions (cf. Equation (11)).

In Figure 3, the fraction $f_{\rm inf}$ is plotted against the stellar mass; the shaded areas reflect the uncertainties in chemical abundance and stellar efficiency. In the case of LTGs, the resulting fraction $f_{\rm inf} \approx 0.9$–1.3 is very close to 1, except in a limited mass range $M_\star \sim 3$–$10 \times 10^9\,M_\odot$, wherein a maximum value of $\approx$1.7 is reached; however, $f_{\rm inf} \lesssim 1$ is allowed at the 1σ level.

For ETGs, the resulting infall fraction reaches a maximum $f_{\rm inf} \approx 0.7$ around $M_\star \approx 3 \times 10^{10}\,M_\odot$ and then declines at larger masses due to the combined decrease in efficiency and increase in metallicity, as shown in Figure 2. However, an infall fraction constant with mass $f_{\rm inf} \approx 0.3$–0.4 is allowed at 1σ.

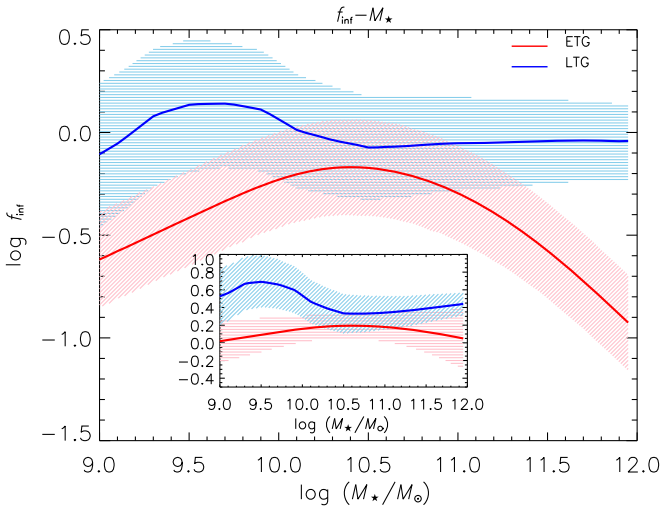

Figure 3. Inferred baryon infalling fraction $f_{\rm inf}$ for ETGs (red) and LTGs (blue). The shaded areas indicate the 1σ uncertainty calculated by taking into account the scatter of the parameters entering Equation (11). In the inset, we plot the quantity $y_Z\, f_\star^{-2/3+s}\, Z_\star^{-s}\, M_\star^{0.15}$ together with its 1σ uncertainty (shaded areas; see the text for details).

Interestingly, the fraction of the inflowing gas that is then removed by feedback $M_{\rm out}/M_{\rm inf}$ is always larger than 70% for LTGs, while it is substantially lower for ETGs (dashed lines in top panel of Figure 4). By contrast, the fraction of inflowing mass eventually retained into stars $M_\star/M_{\rm inf}$ is larger for ETGs, reaching 60% (solid lines in top panel of Figure 4). This reflects the dilution needed for LTGs to keep the stellar metallicity low even in the presence of a higher star formation efficiency.

The bottom panel in Figure 4 shows that only a small fraction of metals produced by stars are retained within the galaxy (i.e., in stars, ISM, and dust). We exclude the CGM from the budget because it does not enter into the galaxy mass and metal balances, though its composition carries some relevant information on complex inflow/outflow processes (see Peeples et al. 2014). For LTGs, such a fraction is $\approx$20%–30%, almost constant with stellar mass, as found by Peeples et al. (2014) for a large sample of spiral galaxies. By contrast, for ETGs, we find that the fraction is increasing with stellar mass, reaching $\approx$60%.

In Figure 5 (top panel), we illustrate the relation between specific angular momentum and stellar mass predicted in Equation (5) for LTGs and ETGs; this constitutes our main result. The differences in the inflowing fraction $f_{\rm inf}$, the efficiencies $f_\star$, and the formation redshift cooperate to yield distinct loci in the angular momentum versus stellar mass plane for the two galaxy types (cf. Equation (5)). To highlight the relevant dependencies, it is worth noticing that the handy approximation $f_{\rm inf} \approx y_Z\, f_\star / \langle Z_\star \rangle$ holds for both galaxy types. By plugging it into Equation (5), the specific angular momentum is seen to scale as

$$j_\star \propto \lambda\, f_j\, f_\star^{-2/3+s}\, Z_\star^{-s}\, M_\star^{2/3}; \qquad (15)$$

where λ is independent of the host halo mass and is assumed not to introduce additional dependence on the stellar mass. The inset of Figure 3 shows that the product $y_Z\, f_\star^{-2/3+s}\, Z_\star^{-s}\, M_\star^{0.15} \approx$ const. is different in normalization for each galaxy type but nearly independent of $M_\star$ for both (within the 1σ uncertainty). Since

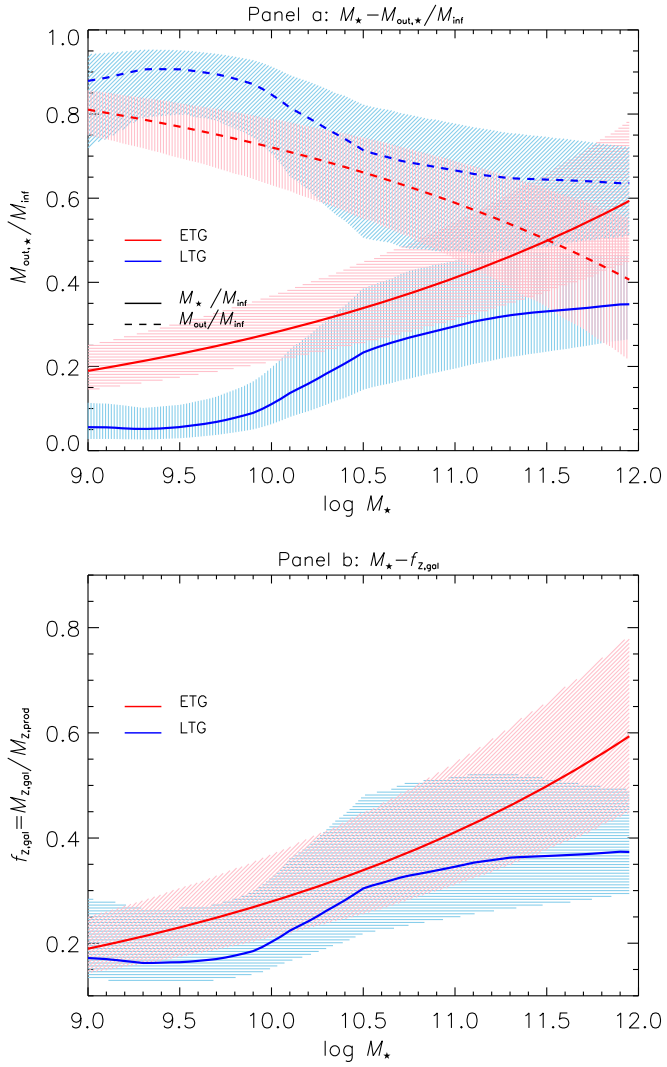

Figure 4. Top panel: stellar mass fraction $M_\star/M_{\rm inf}$ (solid lines) and ejected mass fraction $M_{\rm out}/M_{\rm inf}$ (dashed lines) for ETGs (red) and LTGs (blue). Bottom panel: fraction of metals retained in galaxies $f_{\rm Z,gal} \equiv M_{\rm Z,gal}/M_{\rm Z,prod}$. The shaded areas explicitly show the 1σ uncertainties of the estimates.

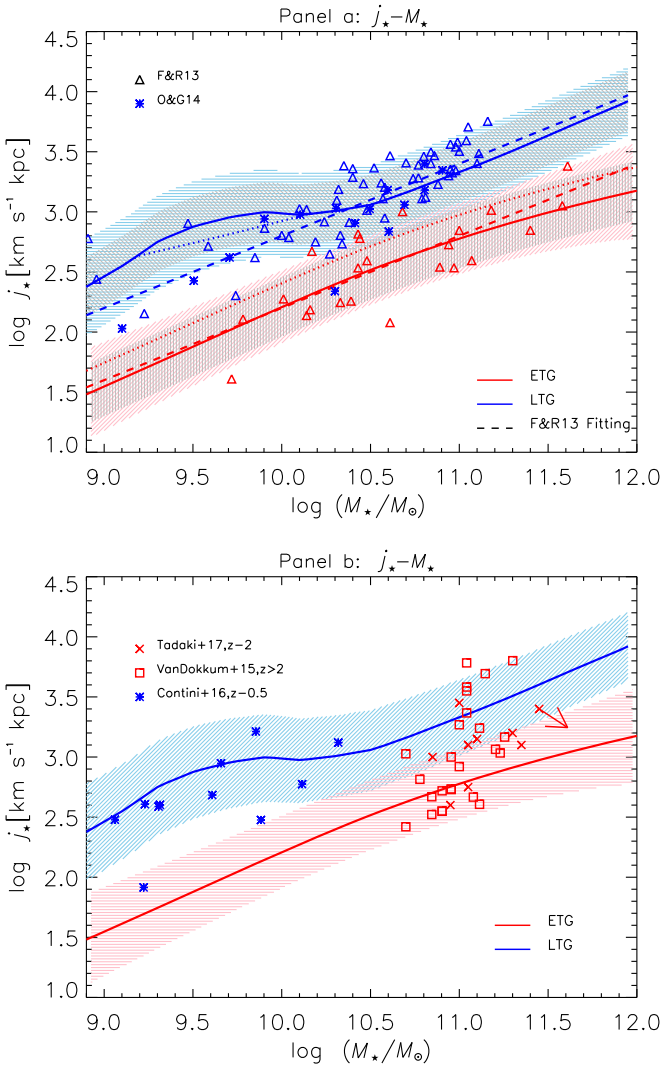

Figure 5. Specific angular momentum $j_\star$ vs. the stellar mass $M_\star$ for ETGs (red lines) and LTGs (blue lines). The blue solid lines are the result for LTGs with a retention fraction $f_j \approx 1$; the dotted blue line applies when limiting the infall fraction $f_{\rm inf} \leqslant 1$. The red solid lines are the result for ETGs taking into account stellar mass growth by dry mergers and a retention fraction $f_j \approx 0.64$; the red dotted line refers to $f_j \approx 1$. In the top panel, dashed lines represent the fitting formula $j_\star \propto M_\star^{0.6}$ adopted by Fall & Romanowsky (2013). The colored shaded areas indicate the 1σ uncertainty calculated by taking into account the variances of the parameters in Equation (5), while the gray shaded areas include only the intrinsic variance in the halo spin parameter λ measured from numerical simulations. The blue and red triangles are data from Fall & Romanowsky (2013) for LTGs and ETGs, respectively. The blue stars are data for local spiral galaxies from Obreschkow & Glazebrook (2014). In the bottom panel, data for star-forming compact galaxies at $z \approx 2$ are reported. Red squares are from van Dokkum et al. (2015), and red crosses are from Tadaki et al. (2017). Data for disk galaxies at $z \approx 0.5$ from Contini et al. (2016) are shown as blue stars. The red arrow explicitly shows the expected evolving direction of the high-z ETG progenitors after considering the growth in stellar mass envisaged by Belli et al. (2014) and $f_j = 0.64$.

$s \sim 1$, the scaling $j_\star \propto f_\star^{1/3}$ applies; hence, the uncertainty in $f_\star$ only marginally contributes to that in $j_\star$.

Our result for LTGs (blue solid lines) well describes the observed $j_\star$ versus $M_\star$ relationship of disks. Note that we allow for $f_{\rm inf} \gtrsim 1$, but we also plot (blue dotted line) the specific angular momentum under the condition $f_{\rm inf} \lesssim 1$; as expected, the estimates are within the respective 1σ uncertainties. Our result for $j_\star$ for LTGs implies a full retention of the initial specific angular momentum, i.e., $f_j \approx 1$. More quantitatively, a Monte Carlo model fitting that takes into account uncertainties in the metallicities, $f_\star$ and $j_\star$, yields $f_j = 1.11^{+0.75}_{-0.44}$. This is consistent within 1σ with the value around 0.8 found by Fall & Romanowsky (2013).

For ETGs, the specific angular momentum (red dotted line) has been computed by using the efficiency at $z \approx 2$ and assuming an absence of evolution in the metal abundance (see Section 4.1 and 4.2). In addition, a shift in stellar mass by a factor of 1.5 has been applied to take into account mass additions by dry mergers at late times (red solid lines; see Section 4.1). Comparison with local data for passive galaxies highlights that some room remains for a possible decrease of the specific angular momentum. Monte Carlo model fitting that takes into account uncertainties in $Z_\star$, $f_\star$, and $j_\star$ yields $f_j = 0.64^{+0.20}_{-0.16}$. The average value may be explained by dry mergers at late times. For instance, if at later epochs the mass of the ETG progenitors is increased because of minor dry mergers with satellite galaxies (e.g., Naab et al. 2009; Belli et al. 2014), then a small decrease of the specific angular momentum can occur. The extent of this decrease is related to the sum of the

initial momentum of the two companion galaxies and their orbital momentum. For a limited mass increase of a factor of 1.5, a small decrease $j_\star \gtrsim 1/1.5 \approx 0.67\, j_{\rm inf}$ is expected, since the randomly oriented angular momentum of the companions partially cancels out (see also Romanowsky & Fall 2012). Note that a value $f_j \lesssim 0.1$, which would be needed to obtain the angular momentum of ETGs from the typical values for LTGs (and for the host halos), is excluded to more than 3σ.

The colored shaded areas in Figure 5 represent the 1σ uncertainty in $j_\star$, which includes the uncertainties in $f_\star$ and metallicity and the intrinsic variance in the exponent s (see shaded areas in Figure 3) and spin parameter λ; the variance in λ actually dominates the overall scatter, as highlighted by the gray areas.

Focusing on the slope of the $j_\star - M_\star$ relation, Romanowsky & Fall (2012) suggested that it can deviate from the expected value of $2/3$, which stems from the definition $M_{\rm vir} = M_\star / f_\star f_b$ and Equation (2); see also Catelan & Theuns (1996). Our results in Figure 5 feature a running slope flatter than but close to $2/3$; specifically, by forcing a single power-law fitting, we get $j_\star \propto M_\star^{0.5}$ for LTGs and $j_\star \propto M_\star^{0.6}$ for ETGs. Interestingly, Fall & Romanowsky (2013) found a slope of around 0.6 for both, as indicated in Figure 5 (top panel) by the dashed lines.

To sum up, for LTGs, the observed metallicity and star formation efficiency imply that the fraction of the available baryons fueling star formation must be close to unity, $f_{\rm inf} \approx 1$. Moreover, the specific angular momentum very well reproduces observations with a retention factor $f_j \approx 1$. By contrast, for ETGs, observations indicate that only a fraction $f_{\rm inf} \approx 0.4$ of the initial baryonic mass $f_b M_{\rm vir}$ must feed star formation; such a fraction of gas is endowed with low specific angular momentum, which turns out to be close to that observed for the stellar component in local passive galaxies. The data leave room for a small decrease $f_j \approx 0.64$ of specific angular momentum due to dry mergers possibly occurring between $z \lesssim 1$ and the present time. Since we find for both galaxy types that the product $f_\star^{-2/3+s}\, Z_\star^{-s}$ only weakly depends on $M_\star$, the slope of the $j_\star$ versus $M_\star$ relationship is close to $2/3$, as observed for both galaxy types.

6. Discussion

In their thoughtful paper, Romanowsky & Fall (2012) reviewed the three most likely explanations for the observed location of ETGs and LTGs in the $j_\star$ versus $M_\star$ plane: (i) outflows of gas by some feedback mechanism or tidal stripping of the galactic halo, (ii) a biased-collapse plus merger scenario, and (iii) pure merger-driven evolution of LTGs into ETGs.

We have shown that current data on the star formation efficiency and stellar metallicity naturally imply different infalling gas fractions for LTGs and ETGs, with average values of $f_{\rm inf} \approx 1$ and 0.4, respectively. These results strongly favor the biased-collapse plus merger scenario, and they naturally locate ETGs and LTGs in two distinct loci of the $j_\star$ versus $M_\star$ plane (cf. Figure 5). While such a scenario is likely not the unique explanation for the observed $j_\star$ versus $M_\star$ relationships in ETGs and LTGs, it points out the possibility that the history of star formation, and hence $f_\star$ and $Z_\star$, provides information on the assembly of the host DM halos and their angular momenta. Below, we compare the predictions of the biased-collapse plus merger scenario to additional observational data and numerical simulations.

6.1. The Case of LTGs

For LTGs, we infer $f_{\rm inf} \approx 1$ and show that this value reproduces the observed $j_\star$ versus $M_\star$ relationship, implying full retention of the specific angular momentum $f_j \approx 1$. Such results are in line with the main assumption of the classical framework for disk formation, namely, that disks keep the overall specific angular momentum of their hosting halos (see Fall & Efstathiou 1980; Mo et al. 1998; van den Bosch et al. 2002; Mo & Mao 2004). A slow assembly of LTG disks is supported by the results of Hudson et al. (2015), which showed that the ratio of the star to the halo mass $M_\star/M_{\rm vir}$ stays constant over a long cosmological timescale (from $z \approx 0.7$ to 0.3); this is the crucial epoch for disk formation, as suggested by classical results on chemical and photometric evolution (see Pezzulli & Fraternali 2016). Accurate spectrography for large samples of $z \approx 1$ star-forming galaxies shows that rotationally dominated systems exhibit a specific angular momentum that is lower by factors of 1.5–2 than those of local LTGs with the same stellar mass (see Harrison et al. 2017; Swinbank et al. 2017). However, Contini et al. (2016) presented evidence that LTGs at moderately low $z \sim 0.5$ fall on the local $j_\star$ versus $M_\star$ relationship within 1σ; this possibly suggests a rather weak dependence on the redshift, such as $E(z)^{-1/6}$ (cf. Equation (5); see also Burkert et al. 2016).

The evolution of the angular momentum in galaxies has also been analyzed in Genel et al. (2015) by exploiting the results of the Illustris cosmological simulation (see Genel et al. 2014; Vogelsberger et al. 2014a, 2014b; DeFelippis et al. 2017) and in Sokołowska et al. (2017) using zoom-in simulation for Milky Way–like galaxies. These authors find that local LTGs retain 100% of the specific angular momentum of their parent halos, likely due to enforced specific recipes for feedback and/or metal recycling. Their conclusion is confirmed by the analyses of Zavala et al. (2016) and Lagos et al. (2017) based on the EAGLE numerical simulation (see also Schaye et al. 2015).

All in all, current observations and simulations indicate that feedback mechanisms (stellar winds, supernova explosions, and possibly AGNs) and ISM physics must cooperate to remove material from the galaxy star-forming regions, while cooling processes replace it with metal-poor, high-specific angular momentum gas; the overall outcome is that the metal content in star-forming regions is diluted and kept to low levels, while the specific angular momentum of the disk is increased. All of this occurs on cosmological timescales of order of many Gyr (see Mollá et al. 2016).

6.2. The Case of ETGs

Romanowsky & Fall (2012) pointed out that the biased collapse scenario should be carefully considered in the case of ETGs, which apparently underwent angular momentum loss. Their main reservation toward biased collapse stems from a constraint on the normalization of the stellar specific angular momentum, which scales as $j_\star \propto f_j\, f_\star^{-2/3}$ under the assumption that the relation $j_{\rm vir} \propto M_{\rm vir}^{2/3}$ expected for DM halos (see Catelan & Theuns 1996) transfers to $j_\star \propto M_\star^{2/3}$ for the stellar component. As a consequence, the normalization of the correlation $j_\star$ versus $M_\star$ is constrained to be $f_j\, f_\star^{-2/3} \approx 0.5$

(cf. Equations (15) and (16) in Romanowsky & Fall 2012). For ETGs, they adopted the fitting formula $f_\star$–$M_\star$ from Dutton et al. (2010), obtaining $f_j \approx 0.1$.

By contrast, we demonstrated that the chemistry and star formation efficiency of ETGs imply a small fraction of infalling gas mass $f_{\rm inf} \approx 0.4$. This parameter just quantifies the amount of biased collapse and naturally decreases the normalization of $j_\star$ by a factor of ≈2.5 (since $j_\star \propto f_j\, f_\star^{-2/3}\, f_{\rm inf}^{s}$ with $s \approx 1$). We have shown that a retention fraction $f_j \approx 0.64$ is needed to reproduce observations; this can be accommodated by late-time dry mergers in terms of mass addition $\Delta M_\star/M_\star \lesssim 0.5$.

One of the most relevant predictions of the biased collapse scenario is that the specific angular momentum has been imprinted in the ETG progenitors since the very beginning, with only minor changes related to later evolution in mass and size. This prediction can be tested by computing the angular momentum of the high-z candidate progenitors of ETGs. Among the observed candidates, there are 25 compact star-forming galaxies at $z \approx 2$ that have been studied in detail by van Dokkum et al. (2015). In particular, the observed structural and kinematical data of this optically selected sample allow us to estimate the specific angular momentum of the galaxies by exploiting the approximation of Romanowsky & Fall (2012), $j \approx k_n\, V_{\rm rot}\, R_e$, where n is the Sérsic (1963) index. The median values for the sample are $n \approx 4$ ($k_4 \approx 2.3$), $R_e \approx 1.4$ kpc, and $V_{\rm rot} \approx 340\,{\rm km\,s^{-1}}$, yielding a median value of $j \approx 1000\,{\rm km\,s^{-1}}$ kpc, very close to that observed in local ETGs endowed with a similar stellar mass of $M_\star \approx 10^{11}\,M_\odot$. Figure 5 (bottom panel) illustrates in detail that 18 out of 25 galaxies (70% of the sample) fall within 1σ of the $j_\star$ versus $M_\star$ relationship of local ETGs.

Tadaki et al. (2017) presented estimates of the specific angular momentum for nine optically selected star-forming galaxies at $z \approx 2$ observed with ALMA and detected at 870 μm. In Figure 5 (bottom panel), these galaxies are shown to exhibit a distribution in the $j_\star$ versus $M_\star$ plane similar to that of the galaxies observed by van Dokkum et al. (2015). These results suggest that most of these galaxies are in fact the progenitors of the local ETGs and that their specific angular momentum is imprinted at the epoch of formation with only minor subsequent changes, as predicted by our scenario. We stress the importance of analyzing larger galaxy samples in order to further test this conclusion.

It is also interesting to compare these observational findings to the outcomes of recent numerical simulations, such as Illustris (see Genel et al. 2014, 2015; Vogelsberger et al. 2014a, 2014b). For LTGs, Genel et al. (2015) found in the simulation a $j_\star$ versus $M_\star$ relation similar to the observed local one. For ETGs, the situation is more complex. For a fraction of the galaxies, namely, those with high final values of $j_\star$, the evolution is quite similar to that of LTGs. By contrast, for simulated ETGs with low final values of $j_\star$, Genel et al. (2015) envisaged two evolutionary paths: (i) rapid initial growth in specific angular momentum combined with a later robust increase in mass by a factor of ∼10 and roughly no change in specific angular momentum, and (ii) a sudden drop of the specific angular momentum mainly imposed by a major merger. These authors also found that radio-mode feedback from AGNs helps in reducing the angular momentum, particularly for high-mass galaxies. In fact, while analyzing the EAGLE simulation (see Schaye et al. 2015), Lagos et al. (2017) put forward the possibility that even early star formation followed by rapid quenching can be effective in producing low-angular-momentum galaxies.

All in all, the analyses of simulated ETGs by Zavala et al. (2016) and Lagos et al. (2017) support a strong relation between the specific angular momentum of the stars and DM in the inner star-forming region. Future data on the specific angular momentum of massive high-z galaxies will provide a crucial test for this scenario and a robust benchmark for next-generation numerical simulations of galaxy formation.

In the biased collapse scenario, the feedback (stellar and AGN) is a key process, since it partially offsets cooling and regulates the fraction of inflowing gas. More specifically, in the case of ETGs, AGN feedback is required in order to stop the gas inflow. This yields a high stellar metallicity and pronounced α-enhancement (see Matteucci 1994; Romano et al. 2002; Thomas et al. 2005) and keeps the specific angular momentum low. The relationships between central black hole mass, stellar mass, and velocity dispersion can also be explained in this context (see Silk & Rees 1998; Granato et al. 2001, 2004; Di Matteo et al. 2005; Lapi et al. 2014). The impact of the biased-collapse plus merger scenario on the size evolution of galaxies at high redshift $z \gtrsim 1$ will be discussed in a forthcoming paper.

7. Summary and Conclusions

We have investigated the origin, shape, scatter, and cosmic evolution of the observed relationship between specific angular momentum $j_\star$ and stellar mass $M_\star$ in ETGs and LTGs. Our main findings are summarized as follows.

1. We have exploited the observed star formation efficiency $f_\star$ and chemical abundance $Z_\star$ to infer the fraction $f_{\rm inf}$ of baryons that infall toward the central regions of galaxies (see Section 4). We find $f_{\rm inf} \approx 1$ for LTGs and ≈0.4 for ETGs weakly dependent on $M_\star$ (see Section 5) with an uncertainty of about 0.25 dex.
2. We have highlighted that the infall fraction $f_{\rm inf}$ is the key variable in determining the distinct loci occupied by LTGs and ETGs in the observed $j_\star$ versus $M_\star$ diagram, with ETGs to feature a relatively lower specific angular momentum than LTGs (see Section 5).
3. We have estimated the fraction $f_j \equiv j_\star/j_{\rm inf}$ of the specific angular momentum associated with the infalling gas eventually retained in the stellar component. For LTGs, we have found $f_j \approx 1.1^{+0.75}_{-0.44}$, which is consistent with the results from observations and simulations and matches the standard disk formation picture (see Section 5). For ETGs, we have found $f_j \approx 0.64^{+0.2}_{-0.16}$, which can be explained by a late-time evolution due to dry mergers.
4. We have found that the dependencies of $f_\star$ and $Z_\star$ on $M_\star$ conspire to make $j_\star \propto f_\star^{-2/3+s}\, Z_\star^{-s}$ weakly dependent on the stellar mass, with an overall shape close to $j_\star \propto M_\star^{2/3}$ (see Section 5).
5. We have shown that the scatter in the observed $j_\star$ versus $M_\star$ relationship for ETGs and LTGs mainly comes from the intrinsic variance in the halo spin parameter λ, while the uncertainties in star formation efficiency $f_\star$ and stellar metallicity $Z_\star$ are minor contributors (Section 5).
6. We have highlighted that the specific angular momentum $j_\star$ for most (∼70%) of the observed star-forming galaxies at $z \sim 2$ is indeed very close to the local value for ETGs,

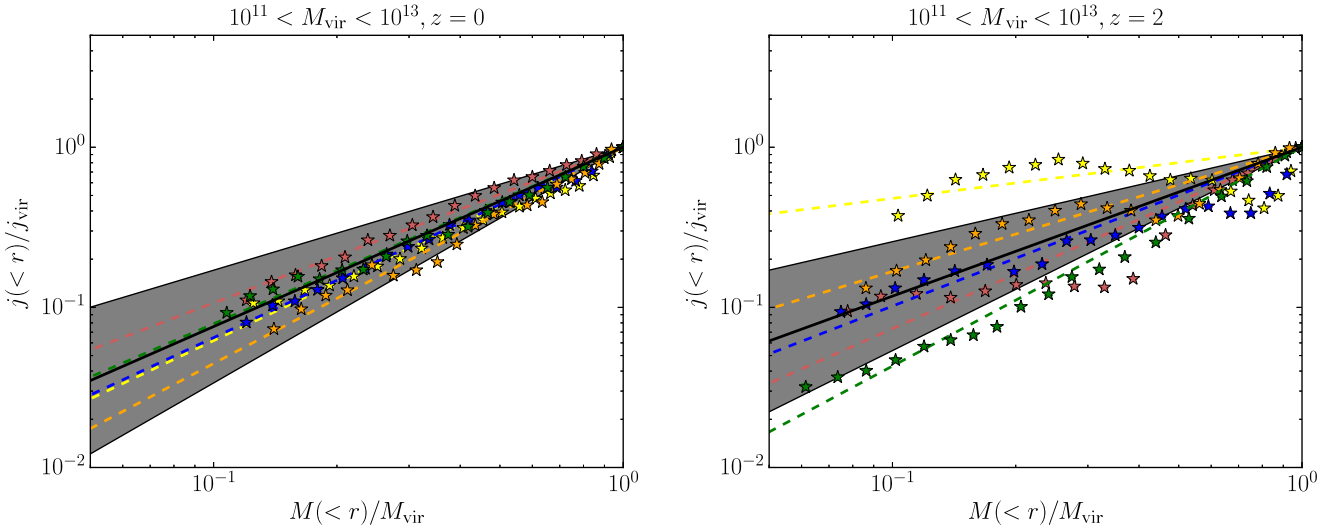

Figure 6. Specific angular momentum vs. mass profile at redshifts $z = 0$ and 2. The lines with stars are the results for several randomly chosen halos in the sample, while the dashed lines are the fits with Equation (17). The black solid lines and the gray shaded areas show the mean profiles and their associated 1σ variance.

as expected in our scenario (see Section 6.2). Recent analyses of state-of-the-art numerical simulations (e.g., Lagos et al. 2017) started to find evidence that early star formation quenching can imprint low specific angular momentum in the stellar component, in good agreement with our scenario based on biased collapse plus mergers.

All in all, we find that, for LTGs, the specific angular momentum steadily changes over cosmological timescales following the external gas inflow, while for ETGs, the specific angular momentum is mainly imprinted in a biased collapse at high redshift and then possibly undergoes a minor decrease due to late-time dry mergers. Thus, we argue that the angular momentum of both galaxy types is mainly imprinted by nature (particularly by the assembly history of their host DM halos) and not nurtured substantially by the environment.

We thank the anonymous referee for valuable suggestions that helped to improve our manuscript. We are grateful to E. Karukes and P. Salucci for stimulating discussions. This work is partially supported by PRIN MIUR 2015 "Cosmology and Fundamental Physics: Illuminating the Dark Universe with Euclid." AL acknowledges the RADIOFOREGROUNDS grant (COMPET-05-2015, agreement number 687312) of the European Union Horizon 2020 research and innovation program. HYW is supported by NSFC (11522324, 11421303).

Appendix A
The Specific Angular Momentum in Spherical Shells of Halos

In this appendix, we use state-of-the-art, high-resolution N-body simulations to investigate the distribution of the specific angular momentum profile within DM halos as a function of mass and redshift.

A.1. Simulation and Halo Identification

We exploit an N-body simulation based on the Gadget-2 code (Springel 2005). The simulation adopted a flat ΛCDM cosmological model from WMAP9 constraints (Hinshaw et al. 2013) with $\Omega_\Lambda = 0.718$, $\Omega_M = 0.282$, $\Omega_b = 0.046$, $h = H_0/100\,{\rm km\,s^{-1}\,Mpc^{-1}} = 0.697$, $\sigma_8 = 0.817$, and $n_s = 0.96$. The CDM density field is traced by 2048^3 particles, each with mass $m_{\rm p} \approx 7.29 \times 10^7\,M_\odot\,h^{-1}$, from $z = 120$ to 0 in a cubic box of a side length $200\,{\rm Mpc}\,h^{-1}$. The gravitational force is softened isotropically on a comoving length scale of $2\,h^{-1}$ kpc (Plummer equivalent). We have 100 snapshots from $z = 20$ to 0 equally spaced in the logarithm of the expansion factor.

The DM halos are identified with the FOF group algorithm (Davis et al. 1985) and a linking length of $0.2\,b$, where b is the mean interparticle separation. We resolve all groups with at least 20 particles. Furthermore, we run SUBFIND (Springel et al. 2001) to acquire the self-bound subhalo catalog for each snapshot. We define the halo mass as the mass contained in a spherical region (centered on the dominant subhalo particle with the minimum gravitational potential) with an average density of $200\,\rho_{\rm crit}$. In the calculation, we take the halo mass range $M_{\rm vir} \sim 10^{11}$–$10^{13}\,h^{-1}\,M_\odot$.

A.2. Specific Angular Momentum Profile

Bullock et al. (2001) found a power-law approximation that describes the angular momentum reasonably well:

$$j_z(M) \propto M(<r)^s, \tag{16}$$

where s is roughly distributed over the halos like a Gaussian with average $s = 1.3 \pm 0.3$. Note that $j_z(M)$ is the specific angular momentum projected to the direction of total angular momentum J.

Here, we look for a description of the relation between $j(M)$ and $M(<r)$, where $j(M)$ is the specific angular momentum (unprojected) within the shell with mass $M(<r)$. So, we first divide each halo into shells between $0.1\,r_{\rm vir}$ and $r_{\rm vir}$. Then, in each shell, we calculate the specific angular momentum $j(<r)$ and mass $M(<r)$. Even though $j(<r)$ does not always increase monotonically with $M(<r)$, as shown by the data points in Figure 6, the power-law fitting does provide a useful rendition for the spherical distribution of j on a statistical basis. Thus, we use the formula

$$\frac{j(M)}{j_{\rm vir}} = \left[\frac{M(<r)}{M_{\rm vir}}\right]^s \tag{17}$$

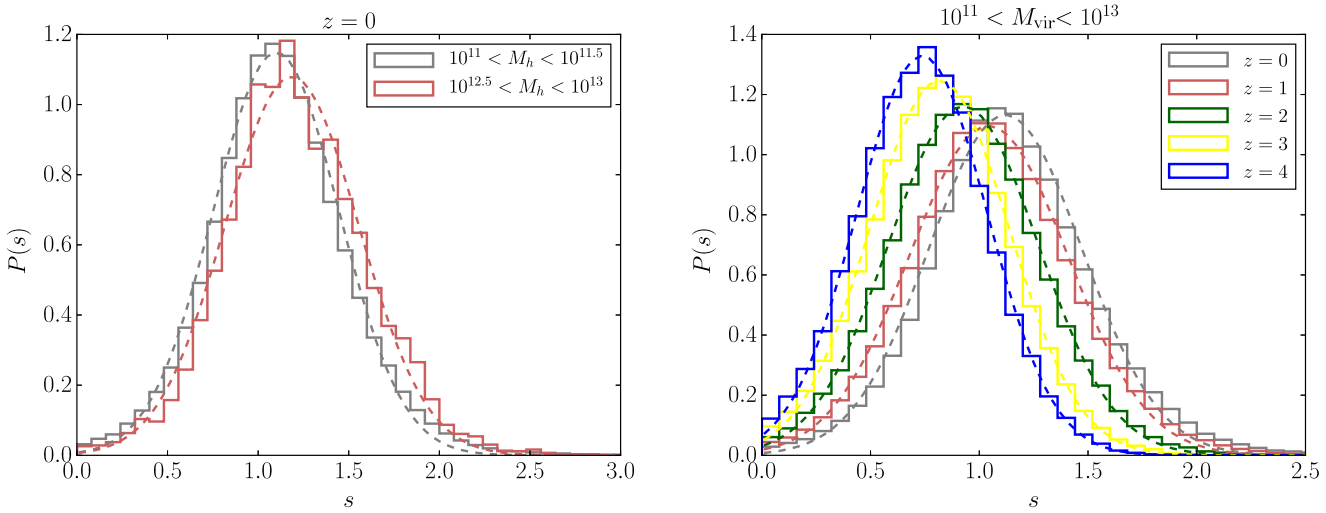

Figure 7. Left panel: distribution of s (power-law parameter in the specific angular momentum profile) for different halo masses at $z = 0$. Right panel: distribution of s at different redshifts for halo masses $M_{\rm vir} \sim 10^{11}$–$10^{13}\,h^{-1}\,M_\odot$. The dashed lines illustrate the Gaussian fits with the fitting parameters given in Table 1.

Table 1
Distribution of s at Different Redshifts

Parameter	$z = 0$	$z = 1$	$z = 2$	$z = 3$	$z = 4$
μ	1.120	1.043	0.927	0.817	0.737
σ	0.352	0.364	0.344	0.320	0.300

Note. A Gaussian function with mean μ and variance σ has been adopted.

to fit our measurements in each halo of our samples. In addition, we check the mass and redshift dependence of the power-law parameter s in Figure 7. We find a very weak dependence on the mass and a decreasing s with increasing z. The fitting parameters for s with varying z are listed in Table 1.

Appendix B
Additional Effects on the Estimate of the Infalling Fraction

In this appendix, we consider two additional effects that can somewhat alter the estimate of the infalling fraction $f_{\rm inf}$ discussed in Section 3.

The first effect concerns the metallicity of the infalling gas, which was neglected in Section 3. We now suppose that the gas mass $M_{\rm inf}$ infalling toward the central galaxy region is endowed with a metallicity $\langle Z_{\rm inf}\rangle$. Then, the metal conservation Equation (10) must be modified into

$$y_Z\,M_\star + \langle Z_{\rm inf}\rangle\,M_{\rm inf} = M_{Z,\rm gal} + M_{Z,\rm out}, \tag{18}$$

and, along the same lines as Section 3, we find that the infall fraction now reads

$$f_{\rm inf} = \frac{f_\star}{1 - \langle Z_{\rm inf}\rangle/\zeta\,\langle Z_\star\rangle} \times \left(\frac{y_Z}{\zeta\,\langle Z_\star\rangle} - \frac{M_{Z,\rm gal}}{\zeta\,\langle Z_\star\rangle M_\star} + \frac{M_{\rm gal}}{M_\star}\right). \tag{19}$$

This replaces Equation (11) of the main text, which is recovered when $\langle Z_{\rm inf}\rangle \ll \zeta\,\langle Z_\star\rangle$. The metallicity of the infalling gas is likely to be quite small, $\langle Z_{\rm inf}\rangle \lesssim$ a few $10^{-2}\,Z_\odot$, as suggested by various estimates for the intergalactic medium of local and high-redshift systems (for a review, see Madau & Dickinson 2014). Considering that $\zeta\,\langle Z_\star\rangle \gtrsim$ a few $10^{-1}\,Z_\odot$ (cf. Figure 2), the correction to our estimate of $f_{\rm inf}$ is minor.

The second effect concerns the possibility that part of the outflowing gas falls back onto the galaxy, in the way of galactic fountain circulation. We suppose that a fraction $\chi_{\rm rec}$ of the gas mass $M_{\rm out}$ outflown with metallicity $\langle Z_{\rm out}\rangle$ by feedback can fall back to the central galaxy after possible mixing with the metal-poor gas in the outer regions.

The equation for the gas mass actually taking part in the galaxy formation process is now written as

$$M_{\rm inf} = M_{\rm gal} + (1 - \chi_{\rm rec})M_{\rm out}, \tag{20}$$

and the metal mass conservation equation is modified into

$$y_Z\,M_\star + \langle Z_{\rm out}\rangle\,\chi_{\rm rec}\,M_{\rm out} = M_{Z,\rm gal} + \langle Z_{\rm out}\rangle\,M_{\rm out}. \tag{21}$$

With respect to the equations in the main text, this amounts to a redefinition of the outflowing gas mass from $M_{\rm out}$ into $(1 - \chi_{\rm rec})M_{\rm out}$. It is apparent that, in a one-zone model like that considered here, galactic fountain circulation does not affect the final value of $f_{\rm inf}$, which turns out to be unchanged with respect to Equation (11). As a matter of fact, in detailed and spatially resolved chemical evolution approaches, the galactic fountain is relevant in time delaying and spatially displacing metals (e.g., Spitoni et al. 2013).

References

Aversa, R., Lapi, A., de Zotti, G., Shankar, F., & Danese, L. 2015, ApJ, 810, 74
Barnes, J., & Efstathiou, G. 1987, ApJ, 319, 575
Behroozi, P. S., Conroy, C., & Wechsler, R. H. 2010, ApJ, 717, 379
Behroozi, P. S., Wechsler, R. H., & Conroy, C. 2013, ApJ, 770, 57
Belli, S., Newman, A. B., & Ellis, R. S. 2014, ApJ, 783, 117
Bett, P., Eke, V., Frenk, C. S., et al. 2007, MNRAS, 376, 215
Böhringer, H. 2014, MmSAI, 85, 396
Bournaud, F. 2016, ASSL, 418, 355
Bournaud, F., Elmegreen, B. G., & Elmegreen, D. M. 2007, ApJ, 670, 237
Bower, R. G., Lucey, J. R., & Ellis, R. S. 1992, MNRAS, 254, 601
Bressan, A., Granato, G. L., & Silva, L. 1998, A&A, 332, 135
Brook, C. B., Stinson, G., Gibson, B. K., et al. 2012, MNRAS, 419, 771
Bullock, J. S., Dekel, A., Kolatt, T. S., et al. 2001, ApJ, 555, 240
Burkert, A., Förster Schreiber, N. M., Genzel, R., et al. 2016, ApJ, 826, 214
Catelan, P., & Theuns, T. 1996, MNRAS, 282, 436

Chabrier, G. 2003, PASP, 115, 763
Chiappini, C., Matteucci, F., & Gratton, R. 1997, ApJ, 477, 765
Choi, J., Conroy, C., Moustakas, J., et al. 2014, ApJ, 792, 95
Citro, A., Pozzetti, L., Moresco, M., & Cimatti, A. 2016, A&A, 592, A19
Cole, S., Lacey, C. G., Baugh, C. M., & Frenk, C. S. 2000, MNRAS, 319, 168
Contini, T., Epinat, B., Bouché, N., et al. 2016, A&A, 591, A49
Davies, R. L., & Illingworth, G. 1983, ApJ, 266, 516
Davis, M., Efstathiou, G., Frenk, C. S., & White, S. D. M. 1985, ApJ, 292, 371
DeFelippis, D., Genel, S., Bryan, G., & Fall, S. M. 2017, arXiv:1703.03806
Del Popolo, A. 2016, Ap&SS, 361, 222
Di Matteo, T., Springel, V., & Hernquist, L. 2005, Natur, 433, 604
Doroshkevich, A. G. 1970, Ap, 6, 320
Dutton, A. A., Conroy, C., van den Bosch, F. C., Prada, F., & More, S. 2010, MNRAS, 407, 2
Dutton, A. A., & van den Bosch, F. C. 2012, MNRAS, 421, 608
Efstathiou, G., & Jones, B. J. T. 1979, MNRAS, 186, 133
Efstathiou, G., & Jones, B. J. T. 1980, ComAp, 8, 169
Eke, V., Efstathiou, G., & Wright, L. 2000, MNRAS, 315, L18
Fakhouri, O., Ma, C.-P., & Boylan-Kolchin, M. 2010, MNRAS, 406, 2267
Fall, S. M. 1983, in IAU Symp. 100, Internal Kinematics and Dynamics of Galaxies, ed. E. Athanassoula (Besancon: Reidel), 391
Fall, S. M. 2002, in ASP Conf. Ser. 275, Disks of Galaxies: Kinematics, Dynamics and Peturbations, ed. E. Athanassoula, A. Bosma, & R. Mujica (San Francisco, CA: ASP), 389
Fall, S. M., & Efstathiou, G. 1980, MNRAS, 193, 189
Fall, S. M., & Romanowsky, A. J. 2013, ApJL, 769, L26
Feldmann, R. 2015, MNRAS, 449, 3274
Freeman, K. C. 1970, ApJ, 160, 811
Fukugita, M., Hogan, C. J., & Peebles, P. J. E. 1998, ApJ, 503, 518
Fukugita, M., & Peebles, P. J. E. 2004, ApJ, 616, 643
Gallazzi, A., Bell, E. F., Zibetti, S., Brinchmann, J., & Kelson, D. D. 2014, ApJ, 788, 72
Gallazzi, A., Charlot, S., Brinchmann, J., & White, S. D. M. 2006, MNRAS, 370, 1106
Gallazzi, A., Charlot, S., Brinchmann, J., White, S. D. M., & Tremonti, C. A. 2005, MNRAS, 362, 41
Genel, S., Fall, S. M., Hernquist, L., et al. 2015, ApJL, 804, L40
Genel, S., Vogelsberger, M., Springel, V., et al. 2014, MNRAS, 445, 175
Glazebrook, K., Schreiber, C., Labbé, I., et al. 2017, arXiv:1702.01751
Goddard, D., Thomas, D., Maraston, C., et al. 2017, MNRAS, 466, 4731
Governato, F., Willman, B., Mayer, L., et al. 2007, MNRAS, 374, 1479
Granato, G. L., De Zotti, G., Silva, L., Bressan, A., & Danese, L. 2004, ApJ, 600, 580
Granato, G. L., Silva, L., Monaco, P., et al. 2001, MNRAS, 324, 757
Haffner, L. M., Dettmar, R.-J., Beckman, J. E., et al. 2009, RvMP, 81, 969
Harrison, C. M., Johnson, H. L., Swinbank, A. M., et al. 2017, arXiv:1701.05561
Hinshaw, G., Larson, D., Komatsu, E., et al. 2013, ApJS, 208, 19
Hopkins, P. F., Hernquist, L., Cox, T. J., Keres, D., & Wuyts, S. 2009, ApJ, 691, 1424
Hoyle, F. 1949, in Problems of Cosmical Aerodynamics, The Origin of the Rotations of the Galaxies, ed. J. M. Burgers & H. C. van de Hulst (Dayton, OH: Central Air Documents Office), 195
Huang, K.-H., Fall, S. M., Ferguson, H. C., et al. 2017, ApJ, 838, 6
Hudson, M. J., Gillis, B. R., Coupon, J., et al. 2015, MNRAS, 447, 298
Immeli, A., Samland, M., Gerhard, O., & Westera, P. 2004a, A&A, 413, 547
Immeli, A., Samland, M., Westera, P., & Gerhard, O. 2004b, ApJ, 611, 20
Kriek, M., Conroy, C., van Dokkum, P. G., et al. 2016, Natur, 540, 248
Krumholz, M. R., & Dekel, A. 2012, ApJ, 753, 16
Lagos, C. d. P., Theuns, T., Stevens, A. R. H., et al. 2017, MNRAS, 464, 3850
Lapi, A., Raimundo, S., Aversa, R., et al. 2014, ApJ, 782, 69
Lapi, A., Salucci, P., & Danese, L. 2013, ApJ, 772, 85
Lapi, A., Shankar, F., Mao, J., et al. 2006, ApJ, 650, 42
Leccardi, A., Rossetti, M., & Molendi, S. 2010, A&A, 510, A82
Lonoce, I., Longhetti, M., Maraston, C., et al. 2015, MNRAS, 454, 3912
Macciò, A. V., Dutton, A. A., van den Bosch, F. C., et al. 2007, MNRAS, 378, 55
Macciò, A. V., Dutton, A. A., & van den Bosch, F. C. 2008, MNRAS, 391, 1940
Madau, P., & Dickinson, M. 2014, ARA&A, 52, 415
Maller, A. H., & Dekel, A. 2002, MNRAS, 335, 487
Man, A. W. S., Zirm, A. W., & Toft, S. 2016, ApJ, 830, 89
Mandelbaum, R., Wang, W., Zu, Y., et al. 2016, MNRAS, 457, 3200
Matteucci, F. 1994, A&A, 288, 57
McBride, J., Fakhouri, O., & Ma, C.-P. 2009, MNRAS, 398, 1858
Mo, H., van den Bosch, F. C., & White, S. 2010, Galaxy Formation and Evolution (Cambridge: Cambridge Univ. Press)
Mo, H. J., & Mao, S. 2004, MNRAS, 353, 829
Mo, H. J., Mao, S., & White, S. D. M. 1998, MNRAS, 295, 319
Moffett, A. J., Kannappan, S. J., Berlind, A. A., et al. 2015, ApJ, 812, 89
Mollá, M., Díaz, Á I., Gibson, B. K., Cavichia, O., & López-Sánchez, Á.-R. 2016, MNRAS, 462, 1329
More, S., van den Bosch, F. C., Cacciato, M., et al. 2011, MNRAS, 410, 210
Moster, B. P., Naab, T., & White, S. D. M. 2013, MNRAS, 428, 3121
Naab, T., Johansson, P. H., & Ostriker, J. P. 2009, ApJL, 699, L178
Navarro, J. F., Frenk, C. S., & White, S. D. M. 1996, ApJ, 462, 563
Navarro, J. F., Frenk, C. S., & White, S. D. M. 1997, ApJ, 490, 493
Noguchi, M. 1999, ApJ, 514, 77
Obreschkow, D., & Glazebrook, K. 2014, ApJ, 784, 26
Onodera, M., Carollo, C. M., Renzini, A., et al. 2015, ApJ, 808, 161
Peebles, P. J. E. 1969, ApJ, 155, 393
Peebles, P. J. E. 1971, A&A, 11, 377
Peeples, M. S., Werk, J. K., Tumlinson, J., et al. 2014, ApJ, 786, 54
Persic, M., & Salucci, P. 1992, MNRAS, 258, 14P
Pezzulli, G., & Fraternali, F. 2016, MNRAS, 455, 2308
Planck Collaboration, Ade, P. A. R., Aghanim, N., et al. 2016, A&A, 594, A13
Reddick, R. M., Wechsler, R. H., Tinker, J. L., & Behroozi, P. S. 2013, ApJ, 771, 30
Renzini, A. 2006, ARA&A, 44, 141
Rodríguez-Puebla, A., Avila-Reese, V., Yang, X., et al. 2015, ApJ, 799, 130
Rodríguez-Puebla, A., Behroozi, P., Primack, J., et al. 2016, MNRAS, 462, 893
Romano, D., Silva, L., Matteucci, F., & Danese, L. 2002, MNRAS, 334, 444
Romanowsky, A. J., & Fall, S. M. 2012, ApJS, 203, 17
Schaye, J., Crain, R. A., Bower, R. G., et al. 2015, MNRAS, 446, 521
Sciama, D. W. 1955, MNRAS, 115, 3
Sembach, K. R., Howk, J. C., Ryans, R. S. I., & Keenan, F. P. 2000, ApJ, 528, 310
Sérsic, J. L. 1963, BAAA, 6, 41
Shankar, F., Lapi, A., Salucci, P., De Zotti, G., & Danese, L. 2006, ApJ, 643, 14
Sharma, S., Steinmetz, M., & Bland-Hawthorn, J. 2012, ApJ, 750, 107
Shi, J., Wang, H., & Mo, H. J. 2015, ApJ, 807, 37
Shlosman, I., & Noguchi, M. 1993, ApJ, 414, 474
Silk, J., & Rees, M. J. 1998, A&A, 331, L1
Siudek, M., Małek, K., Scodeggio, M., et al. 2017, A&A, 597, A107
Sokołowska, A., Capelo, P. R., Fall, S. M., et al. 2017, ApJ, 835, 289
Spitoni, E., Matteucci, F., & Marcon-Uchida, M. M. 2013, A&A, 551, A123
Springel, V. 2005, MNRAS, 364, 1105
Springel, V., White, S. D. M., Tormen, G., & Kauffmann, G. 2001, MNRAS, 328, 726
Swinbank, M., Harrison, C., Trayford, J., et al. 2017, arXiv:1701.07448
Tadaki, K.-I., Genzel, R., Kodama, T., et al. 2017, ApJ, 834, 135
Takase, B., & Kinoshita, H. 1967, PASJ, 19, 409
Thomas, D., Maraston, C., Bender, R., & Mendes de Oliveira, C. 2005, ApJ, 621, 673
Thomas, D., Maraston, C., Schawinski, K., Sarzi, M., & Silk, J. 2010, MNRAS, 404, 1775
Trujillo, I., Ferreras, I., & de La Rosa, I. G. 2011, MNRAS, 415, 3903
Tumlinson, J., Thom, C., Werk, J. K., et al. 2011, Sci, 334, 948
van den Bosch, F. C., Abel, T., Croft, R. A. C., Hernquist, L., & White, S. D. M. 2002, ApJ, 576, 21
van den Bosch, F. C., Burkert, A., & Swaters, R. A. 2001, MNRAS, 326, 1205
van Dokkum, P. G., Nelson, E. J., Franx, M., et al. 2015, ApJ, 813, 23
Velander, M., van Uitert, E., Hoekstra, H., et al. 2014, MNRAS, 437, 2111
Vincenzo, F., Matteucci, F., Belfiore, F., & Maiolino, R. 2016, MNRAS, 455, 4183
Vogelsberger, M., Genel, S., Springel, V., et al. 2014a, Natur, 509, 177
Vogelsberger, M., Genel, S., Springel, V., et al. 2014b, MNRAS, 444, 1518
Wang, P., & Kang, X. 2017, MNRAS, 468, L123
White, S. D. M. 1984, ApJ, 286, 38
White, S. D. M., & Frenk, C. S. 1991, ApJ, 379, 52
White, S. D. M., & Rees, M. J. 1978, MNRAS, 183, 341
Wojtak, R., & Mamon, G. A. 2013, MNRAS, 428, 2407
Zavala, J., Frenk, C. S., Bower, R., et al. 2016, MNRAS, 460, 4466